Sensorless Control Method for PMSM Based on Frequency-Adaptive Disturbance Observer

Yongsoon Park and Seung-Ki Sul
Department of Electrical and Computer Engineering
Seoul National University, Seoul, Korea

***Abstract*—The rotor angle can be estimated from the stator flux in permanent magnet synchronous motor (PMSM). Although integrations are essential to estimate the stator flux from the voltages and currents in the stationary reference frame, disturbances can arise in the process of integrations due to practical reasons. In this paper, a frequency-adaptive disturbance observer has been proposed to remove the disturbances in estimating the stator flux and to enhance the accuracy of the rotor angle estimation. The design and utilization of the proposed observer are detailed under the consideration of its application to the practical system driving PMSM. The performance of the proposed sensorless method has been mainly assessed through experiments at low speed operations, where the sensorless drive of PMSM is regarded as being extremely difficult without the signal injection.**

I. INTRODUCTION

For high performance servo drive, the rotor angle of permanent magnet synchronous motor (PMSM) should be detected without time delay. The rotor angle indicates the direction of rotor flux originated from the permanent magnet, and the position sensor is normally used to detect it. However, the position sensor may cause some problems related to extended axial length, extra cost, reliability concern, and electromagnetic interference (EMI) of signal.

The sensorless control methods have been discussed for the last few decades to detect the rotor angle without position sensor. Among the sensorless control methods, the high frequency signal injection-based method has been considered as the most robust one in particular at extremely low speed [1]-[2]. However, the injection-based method fundamentally has the demerit of audible noise and additional losses due to the injected signal itself. Furthermore, because the injection signal cannot be infinitesimal for the clear detection of rotor angle [8], the additional voltage for the injection takes voltage of pulse width modulation (PWM) inverter, and the maximum available voltage to drive the motor would be reduced. Moreover, if the spatial saliency of inductance does not exist in the motor, the injection-based method cannot be used for the sensorless control.

Meanwhile, the detection of rotor angle can be based on the circuital modeling of motor, which is commonly called as the back electromotive force (EMF) based method [3]-[5]. This back-EMF based method can overcome the most demerit of the injection-based method if the rotating speed is high enough to make the back-EMF detectable. However, the back-EMF must be infinitesimal at extremely low speed even if it is accurately estimated. That is, any trivial noise near zero speed can be fatal in the back-EMF based method. This weakness confines the broad application of the back-EMF based method.

The sensorless control can be also accomplished with the other model, based on the stator flux of PMSM [6]-[7]. Contrary to the back-EMF, the stator flux is not disappeared even at zero speed unless the rotor flux is completely offset by stator currents. However, since the stator flux cannot be directly measured in ordinary drive system, how to measure or estimate the stator flux is the critical issue in the stator flux-based sensorless method. In the literature, even though the current model is combined with the voltage model to accurately estimate the stator flux, the current model has been derived under the assumption of accurate rotor angle and motor parameters. According to the operating condition of PMSM drive system, those assumptions may not be valid.

In this paper, a disturbance observer is newly proposed to replace the current model of stator flux in the stator flux-based sensorless method. In particular, this observer has been proposed to separate unnecessary signals from the signal meaning stator flux while the separation process does not depend on the model of PMSM. Then, this construction would be robust to motor parameter variation. The effectiveness of the proposed sensorless method would be verified through the experimental results.

II. ESTIMATION OF ROTOR ANGLE

The voltage equation of PMSM is given in the stationary reference frame as follows:

$$\begin{bmatrix} v_\alpha \\ v_\beta \end{bmatrix} = \begin{bmatrix} R_s & 0 \\ 0 & R_s \end{bmatrix} \begin{bmatrix} i_\alpha \\ i_\beta \end{bmatrix} + \frac{d}{dt} \left\{ \begin{bmatrix} \cos\theta_r & -\sin\theta_r \\ \sin\theta_r & \cos\theta_r \end{bmatrix} \begin{bmatrix} \lambda_d \\ \lambda_q \end{bmatrix} \right\} \quad (1)$$

$$\lambda_d = L_d i_d + \lambda_f, \quad \lambda_q = L_q i_q \quad (2)$$

, where R_s is the stator resistance, and the synchronous d-q inductances are denoted by L_d and L_q, respectively. In addition, λ_f refers to the flux linkage of permanent magnet,

978-1-4799-0336-8/13/$31.00 ©2013 IEEE

and θ_r to the rotor angle. The direct-quadrature axes are indicated by α–β in the stationary reference frame and by d–q in the rotor reference frame, henceforth.

Considering (1), the stator flux can be calculated through integration process as follows:

$$\begin{bmatrix}\lambda_\alpha\\ \lambda_\beta\end{bmatrix}=\int\left(\begin{bmatrix}v_\alpha\\ v_\beta\end{bmatrix}-R_s\begin{bmatrix}i_\alpha\\ i_\beta\end{bmatrix}\right)dt=\begin{bmatrix}\cos\theta_r & -\sin\theta_r\\ \sin\theta_r & \cos\theta_r\end{bmatrix}\begin{bmatrix}\lambda_d\\ \lambda_q\end{bmatrix}. \quad (3)$$

When the synchronous fluxes in (2) are inserted into (3), the stator flux can be derived as

$$\begin{bmatrix}\lambda_\alpha\\ \lambda_\beta\end{bmatrix}=\begin{bmatrix}\cos\theta_r & -\sin\theta_r\\ \sin\theta_r & \cos\theta_r\end{bmatrix}\left\{\begin{bmatrix}\lambda_f+(L_d-L_q)i_d\\ 0\end{bmatrix}+L_q\begin{bmatrix}i_d\\ i_q\end{bmatrix}\right\}. \quad (4)$$

After the coordinate transformation from the d–q reference frame to α–β reference frame is applied to the currents, (5) can be derived from (4):

$$\begin{bmatrix}\lambda_\alpha\\ \lambda_\beta\end{bmatrix}-L_q\begin{bmatrix}i_\alpha\\ i_\beta\end{bmatrix}=\{\lambda_f+(L_d-L_q)i_d\}\begin{bmatrix}\cos\theta_r\\ \sin\theta_r\end{bmatrix}=\lambda_{em}\begin{bmatrix}\cos\theta_r\\ \sin\theta_r\end{bmatrix}. \quad (5)$$

Considering (3) and (5), the information related to rotor angle can be obtained with the voltages and currents in the α–β frame because the left-side flux in (5) can be deduced from (3). Unless λ_{em} in (5) becomes null depending on operating conditions, the rotor angle can be directly calculated as

$$\theta_r=\tan^{-1}\left(\frac{\lambda_\beta-L_q i_\beta}{\lambda_\alpha-L_q i_\alpha}\right)=\tan^{-1}\left(\frac{\lambda_{\beta r}}{\lambda_{\alpha r}}\right). \quad (6)$$

The effectiveness of (6) can be simply checked by inserting a maximum allowable current into i_d of (5) and calculating the corresponding magnitude of λ_{em}. If λ_{em} is always positive under operation, (6) can be used to calculate the rotor angle. For the most cases of PMSM, λ_{em} may have positive value even with the maximum i_d.

It is noticeable that the procedure to detect the rotor angle by (6) is not based on any assumptions pertaining to estimated angle and speed, which are common in the sensorless control methods [1]-[7]. The motor parameters of R_s and L_q have to be known for the angle estimation while the others, L_d and λ_f, do not by virtue of (6).

In addition to the detection of rotor angle, the rotating speed can be needed for speed control of PMSM. This speed can be estimated through type 2 system (T2S) shown in Fig. 1 [9], [11]. Moreover, because any noise over the bandwidth of T2S can be filtered out in the angle estimation as well, the filtered angle by T2S is preferred as the estimated angle in this paper rather than the angle directly from (6).

III. Diturbance Observer for Flux Estimation

For the calculation of the rotor angle by (6), the flux estimation is crucial. In this flux estimation, it is inevitable to use the integrations in (3). However, the application of integrator in the signal processing may suffer from disturbances.

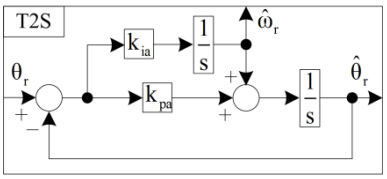

Fig. 1. Type 2 system (T2S) for the estimation of angle and speed.

Namely, if additional treatment is absent, the estimated stator fluxes in the α–β frame may contain some disturbances. These disturbances can arise from the practical reasons such as initialization errors of integrators, impulse noises of sensors, and quantization errors in digital system. Whatever the reason may be, these types of disturbances should be offset for the accurate estimation of rotor angle and speed.

A. State Equation to Design the Disturbance Observer

When λ_m refers to the magnitude of stator flux in the α–β frame, the stator flux estimated by (3) in a practical system can be modeled as

$$\begin{bmatrix}\lambda_{\alpha 1}\\ \lambda_{\beta 1}\end{bmatrix}=\lambda_m\begin{bmatrix}\cos\theta_f\\ \sin\theta_f\end{bmatrix}+\begin{bmatrix}D_\alpha\\ D_\beta\end{bmatrix} \quad (7)$$

, where $\lambda_{\alpha 1}$ and $\lambda_{\beta 1}$ represent the initially estimated stator fluxes based on (3), and the disturbances are denoted by D_α and D_β. In addition, θ_f means the stator flux angle.

When λ_m and the disturbances are assumed to be step-varying, the derivative of (7) can be derived as

$$\frac{d}{dt}\begin{bmatrix}\lambda_{\alpha 1}\\ \lambda_{\beta 1}\end{bmatrix}\approx\omega_f\lambda_m\begin{bmatrix}-\sin\theta_f\\ \cos\theta_f\end{bmatrix}=\omega_f\begin{bmatrix}D_\beta-\lambda_{\beta 1}\\ \lambda_{\alpha 1}-D_\alpha\end{bmatrix} \quad (8)$$

, where ω_f means the rotating speed of stator flux.

Based on (8), the state equation on the estimated stator flux can be derived as (9):

$$\frac{d}{dt}\lambda_{\alpha\beta D}=\begin{bmatrix}0 & -\omega_f & 0 & \omega_f\\ \omega_f & 0 & -\omega_f & 0\\ 0 & 0 & 0 & 0\\ 0 & 0 & 0 & 0\end{bmatrix}\cdot\lambda_{\alpha\beta D}=A_m\lambda_{\alpha\beta D} \quad (9\text{-a})$$

$$\lambda_{\alpha\beta 1}=\begin{bmatrix}\lambda_{\alpha 1}\\ \lambda_{\beta 1}\end{bmatrix}=\begin{bmatrix}1 & 0 & 0 & 0\\ 0 & 1 & 0 & 0\end{bmatrix}\cdot\lambda_{\alpha\beta D}=C_m\lambda_{\alpha\beta D} \quad (9\text{-b})$$

, where $\lambda_{\alpha\beta D}=\begin{bmatrix}\lambda_{\alpha 1} & \lambda_{\beta 1} & D_\alpha & D_\beta\end{bmatrix}^T$. (9-c)

It can be easily confirmed through A_m and C_m in (9) whether the linear system is observable or not [10]. Because the linear system in (9) is observable, a Luenburger observer can be designed as

$$\frac{d}{dt}\hat{\lambda}_{\alpha\beta D}=A_m\hat{\lambda}_{\alpha\beta D}+L_m\cdot[\lambda_{\alpha\beta 1}-C_m\hat{\lambda}_{\alpha\beta D}] \quad (10\text{-a})$$

$$\text{, where } L_m=\begin{bmatrix}p_1 & p_3 & q_1 & q_3\\ p_2 & p_4 & q_2 & q_4\end{bmatrix}^T \quad (10\text{-b})$$

$$\hat{\lambda}_{\alpha\beta D}=\begin{bmatrix}\hat{\lambda}_{\alpha 1} & \hat{\lambda}_{\beta 1} & \hat{D}_{\alpha} & \hat{D}_{\beta}\end{bmatrix}^{T}. \tag{10-c}$$

The hat '^' indicates estimated value hereafter, and the variables in L_m are the observer gains.

B. Gain Settings of the Disturbance Observer

The disturbance observer in (10) features adaptive gains related to ω_f. The similar concept to (10) was proposed in the literature [11]. However, the observer in [11] only considered the case of positive speed. On the other hand, in this paper, the speed reversal of PMSM had to be incorporated in the design of the observer.

For the gain settings, the internal transfer functions of the observer can be discussed. These transfer functions are derived as (11) as explained in [11]:

$$\begin{aligned}\hat{\lambda}_{\alpha 1}&=(A_t\cdot\lambda_{\alpha 1}+E_t\cdot\lambda_{\beta 1})/P_t\\ \hat{\lambda}_{\beta 1}&=(B_t\cdot\lambda_{\alpha 1}+F_t\cdot\lambda_{\beta 1})/P_t\\ \hat{D}_{\alpha}&=(C_t\cdot\lambda_{\alpha 1}+G_t\cdot\lambda_{\beta 1})/P_t\\ \hat{D}_{\beta}&=(D_t\cdot\lambda_{\alpha 1}+H_t\cdot\lambda_{\beta 1})/P_t\end{aligned} \tag{11}$$

, where all transfer functions in (11) are detailed with

$$\begin{aligned}A_t&=s^3p_1+s^2(p_1p_4-p_2p_3+\omega_f(q_3-p_3))\\&+s\cdot\omega_f(p_2q_1-p_1q_2+p_4q_3-p_3q_4+\omega_fq_1)+\omega_f^2(q_1q_4-q_2q_3)\end{aligned} \tag{12-a}$$

$$B_t=s^3p_3+s^2\omega_f(p_1-q_1)+s\cdot\omega_f^2q_3 \tag{12-b}$$

$$\begin{aligned}C_t&=s^3q_1+s^2(p_4q_1-p_3q_2)\\&+s\cdot\omega_f(p_2q_1-p_1q_2+\omega_fq_1)+\omega_f^2(q_1q_4-q_2q_3)\end{aligned} \tag{12-c}$$

$$\begin{aligned}D_t&=s^3q_3+s^2(p_4q_3-p_3q_4)\\&+s\cdot\omega_f(q_3(p_2-q_2)+q_4(q_1-p_1)+\omega_fq_3)\end{aligned} \tag{12-d}$$

$$E_t=s^3p_2+s^2\omega_f(q_4-p_4)+s\cdot\omega_f^2q_2 \tag{12-e}$$

$$\begin{aligned}F_t&=s^3p_4+s^2(p_1p_4-p_2p_3+\omega_f(p_2-q_2))\\&+s\cdot\omega_f(p_2q_1-p_1q_2+p_4q_3-p_3q_4+\omega_fq_4)+\omega_f^2(q_1q_4-q_2q_3)\end{aligned} \tag{12-f}$$

$$\begin{aligned}G_t&=s^3q_2+s^2(p_1q_2-p_2q_1)\\&+s\cdot\omega_f(q_1(p_4-q_4)+q_2(q_3-p_3)+\omega_fq_2)\end{aligned} \tag{12-g}$$

$$\begin{aligned}H_t&=s^3q_4+s^2(p_1q_4-p_2q_3)\\&+s\cdot\omega_f(p_4q_3-p_3q_4+\omega_fq_4)+\omega_f^2(q_1q_4-q_2q_3)\end{aligned} \tag{12-h}$$

$$\begin{aligned}P_t&=s^4+s^3(p_1+p_4)+\omega_f^2(q_1q_4-q_2q_3)\\&+s^2(\omega_f^2+p_1p_4-p_2p_3+\omega_f(p_2-p_3+q_3-q_2))\\&+s\cdot\omega_f(p_2q_1-p_1q_2+p_4q_3-p_3q_4+\omega_f(q_1+q_4))\end{aligned}. \tag{13}$$

As shown in (12) and (13), the properties of internal transfer functions are dependent on ω_f, which is the angular frequency of stator flux. Then, the observer poles are in danger of being moved into the right-half plane if ω_f is reversed, which leads to unstable operations. To neutralize the influence of frequency reversal, the observer gains can be adjusted according to

$$p_1-q_1=k_1\omega_f \tag{14-a}$$

$$p_2-q_2=k_2\omega_f \tag{14-b}$$

$$q_3-p_3=k_3\omega_f \tag{14-c}$$

$$q_4-p_4=k_4\omega_f \tag{14-d}$$

$$p_2q_1-p_1q_2+p_4q_3-p_3q_4=k_5\omega_f. \tag{14-e}$$

By the setting of (14), ω_f only appears as the form of its square in the coefficients of the internal transfer functions. That is, the poles and zeros at a certain speed are the same with those at the reversed speed. Then, the observer poles can be placed by considering the positive case only. In addition, the condition of (15) can be adopted to make the observer structure symmetric in the α–β frame:

$$p_1=p_4,\ p_2=-p_3,\ q_1=-q_4=0,\ q_2=-q_3,\ k_2=k_3,\ k_4=-k_1. \tag{15}$$

If all the roots of (13), the observer poles, are placed at the distance of $|\omega_f|$ on the negative real axis of Laplace domain, the observer gains are finally determined as

$$\begin{cases}p_1=p_4=2|\omega_f|\\ p_2=-p_3=-\omega_f\\ q_1=-q_4=0\\ q_2=-q_3=-\omega_f\end{cases}. \tag{16}$$

When the gains in (16) are used, the transfer functions pertaining to the disturbances are derived as

$$\begin{cases}\hat{D}_{\alpha}=\dfrac{\omega_f^2}{s^2+2|\omega_f|s+\omega_f^2}\lambda_{\alpha 1}+\dfrac{-\omega_f s}{s^2+2|\omega_f|s+\omega_f^2}\lambda_{\beta 1}\\ \hat{D}_{\beta}=\dfrac{\omega_f s}{s^2+2|\omega_f|s+\omega_f^2}\lambda_{\alpha 1}+\dfrac{\omega_f^2}{s^2+2|\omega_f|s+\omega_f^2}\lambda_{\beta 1}\end{cases}. \tag{17}$$

Considering (17), the observer serves as low-pass filters to $\lambda_{\alpha 1}$ and $\lambda_{\beta 1}$ in each axis while it particularly offers simultaneous notch-filtering at ω_f via the cross-couplings. To detail the cross-coupling effect, the flux components at ω_f can be discussed separately since superposition establishes in linear systems. And, the flux components at ω_f can be described with (18) as per the definition of the α–β frame:

$$\begin{bmatrix}\lambda_{\alpha 1}(t)\\ \lambda_{\beta 1}(t)\end{bmatrix}=\begin{bmatrix}\lambda_m\cos(\omega_f t)\\ \lambda_m\sin(\omega_f t)\end{bmatrix}\xrightarrow{\mathcal{L}}\lambda_{\beta 1}(s)=\frac{\omega_f}{s}\lambda_{\alpha 1}(s). \tag{18}$$

When the relationship of (18) is employed, the transfer functions in (17) can be changed into

$$\begin{cases}\hat{D}_{\alpha}=\left(\dfrac{\omega_f^2}{s^2+2|\omega_f|s+\omega_f^2}+\dfrac{-\omega_f s}{s^2+2|\omega_f|s+\omega_f^2}\cdot\dfrac{\omega_f}{s}\right)\cdot\lambda_{\alpha 1}\\ \hat{D}_{\beta}=\left(\dfrac{\omega_f s}{s^2+2|\omega_f|s+\omega_f^2}\cdot\dfrac{s}{\omega_f}+\dfrac{\omega_f^2}{s^2+2|\omega_f|s+\omega_f^2}\right)\cdot\lambda_{\beta 1}\end{cases}. \tag{19}$$

Then, by replacing s with $j\omega_f$ in (19), it is confirmed that the frequency responses become null at ω_f. In other words, the component at ω_f cannot be reflected into the estimation of disturbances as if notch filters work. This notch filtering at ω_f is very useful to clearly extract the disturbances because the largest ac components of $\lambda_{\alpha 1}$ and $\lambda_{\beta 1}$ normally appear at that frequency.

C. Disturbance Observer for Stator Flux Estimation

The block diagram of the proposed disturbance observer can be depicted as shown in Fig. 2 when the gain settings in (16) are applied to (10). Because ω_f cannot be measured in the sensorless control system, its estimated one is used to update the adaptive gains instead. In addition, it is evident in Fig. 2 that all the integrations in the proposed observer are stopped when ω_f is zero, which coincides with the natural property of stator flux at standstill.

Considering (7), the stator flux required for the angle estimation can be calculated by

$$\begin{bmatrix}\lambda_{\alpha 2}\\ \lambda_{\beta 2}\end{bmatrix}=\begin{bmatrix}\lambda_{\alpha 1}-\hat{D}_\alpha\\ \lambda_{\beta 1}-\hat{D}_\beta\end{bmatrix}=\hat{\lambda}_m\begin{bmatrix}\cos\hat{\theta}_f\\ \sin\hat{\theta}_f\end{bmatrix}. \tag{20}$$

If $\lambda_{\alpha 2}$ and $\lambda_{\beta 2}$ in (20) are inserted into (6) instead of λ_α and λ_β, the rotor angle can be directly calculated. As mentioned earlier, this direct angle is utilized as the input to T2S shown in Fig. 1. As one output of T2S, the estimated angular frequency is fed-back to the disturbance observer to update the frequency-adaptive gains in Fig. 2. If the feedback frequency to the observer is not accurate, the stop-band of the notch filtering deviates from the actual frequency of stator flux. This deviation may cause some oscillations in the estimation of the disturbances. Therefore, the bandwidth of the T2S should be carefully determined in order to filter out fluctuations in the speed estimation under the proper dynamics to track actual load variations.

The subtraction of disturbance in (20) would contribute to the accuracy enhancement in the estimation of stator flux. However, this subtraction cannot reduce the cumulative amount of disturbances in the integrators. If this accumulation is not obstructed at all, the ratio of ac flux to dc flux in $\lambda_{\alpha 1}$ and $\lambda_{\beta 1}$ might become infinitesimal. In other words, the resolution of effective ac signals can be lowered as the running time increases. To eliminate this type of risk, the feedback gain of k_{df} is utilized in the flux estimation as described in Fig. 3.

Contrary to the feed-forward calculation in (20), the introduction of k_{df} in Fig. 3 forms closed-loops, which can alter the dynamics to estimate $\lambda_{\alpha 1}$ and $\lambda_{\beta 1}$. Thus, k_{df} should be carefully determined. For the α-axis estimation, (21) can be derived from Fig. 3:

$$\{(v_\alpha^*-\hat{R}_s i_\alpha)-k_{df}\hat{D}_\alpha\}\frac{1}{s}=\lambda_{\alpha 1} \tag{21}$$

, where the asterisk '*' indicates reference value.

Because the estimated disturbances can be expressed with

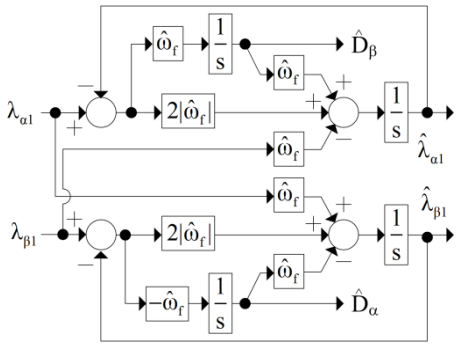

Fig. 2. Proposed disturbance observer.

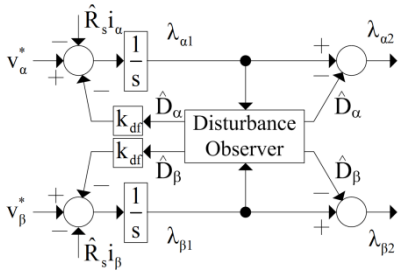

Fig. 3. Flux estimation with disturbance feedback.

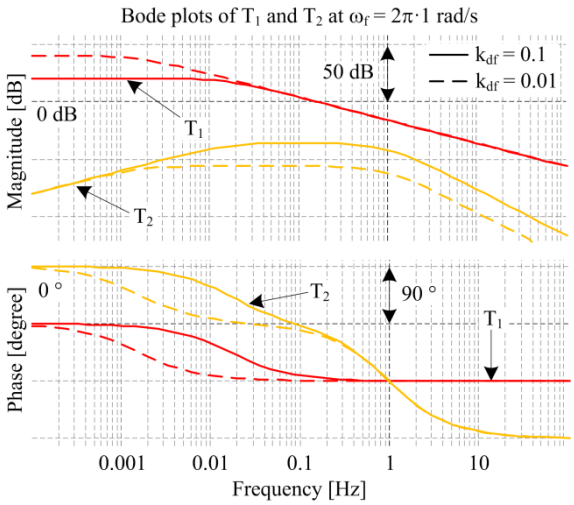

Fig. 4. Influence of feedback gain k_{df}.

respect to $\lambda_{\alpha 1}$ and $\lambda_{\beta 1}$ as shown in (17), equation (21) can be rearranged into (22) by the replacement of $\hat{D}_\alpha$:

$$\begin{aligned}\lambda_{\alpha 1}&=\frac{(s^2+s\cdot 2|\omega_f|+\omega_f^2)(v_\alpha^*-\hat{R}_s i_\alpha)+s\cdot k_{df}\omega_f\cdot\lambda_{\beta 1}}{s^3+s^2 2|\omega_f|+s\cdot\omega_f^2+k_{df}\omega_f^2}\\&=T_1\cdot(v_\alpha^*-\hat{R}_s i_\alpha)+T_2\cdot\lambda_{\beta 1}\end{aligned}. \tag{22}$$

The effect of k_{df} can be explicitly understood through the Bode plots of T_1 and T_2 in (22) as shown in Fig. 4. To draw the figure, the angular frequency of stator flux has been assumed as $2\pi \cdot 1$ rad/s, which is 1 Hz. The analysis is focusing on the α-frame because the case of the β-frame is almost the same.

Considering Fig. 4, from the perspective of T_1, the proposed system in Fig. 3 serves as an integrator in the frequency range larger than k_{df}. When the frequency of concern is getting smaller near null in the Bode plot of Fig. 4, k_{df} plays a role in confining the magnitude of T_1, which can prevent the aforementioned limitless accumulation. In addition, although the undesirable cross-coupling of $\lambda_{\beta 1}$ in (22) is also caused by the feedback loop, its corresponding response T_2 mostly presents small magnitudes.

However, it is necessary to deactivate k_{df} at extremely low speed. This is because the effect of cross-coupling is not negligible any more when ω_f approaches to zero in (22). Moreover, because the effect of k_{df}, in fact, means the distortion of normal integrator, it is needed to restore the original feature of integrator to deal with very slow variation of stator flux near zero speed. The deactivation of k_{df} may not cause the resolution problem if the running time under the deactivation is not too long practically.

IV. Practical Implmentation of Proposed Sensorless Control System

A. Overview of Sensorless Control System

The entire control system for the sensorless drive of PMSM is depicted in Fig. 5. The rotor angle is directly calculated from the stator flux, which is estimated by using the currents and voltage references in the α–β frame. The flux estimation part in Fig. 5 includes (6) in addition to Figs. 2 to 3. The directly calculated angle by (6) is used as the input of two T2Ss, which are T2S-1 and T2S-2.

The bandwidths of T2Ss are differently set according to each purpose. In Fig. 5, the higher bandwidth is assigned for T2S-1 to quickly track the variation of rotor angle with updating the adaptive gains of observer. In contrast, the lower bandwidth is allowed for T2S-2 to make the estimated speed less sensitive to distortions. This damped speed is used for the speed and current controls because their stabilities are vulnerable to the distortions of estimated speed.

B. Compensation Strategies for Practical Implementation

The inverter nonlinearity and digital delay can degrade the estimation accuracy of rotor angle when the voltage references are used for the sensorless drive of PMSM [9]. This is because they can cause the difference between the voltage reference and its pulse-width-modulated output. Even if these sorts of problems may be improved via the direct sensing of pulse-width-modulated outputs [12], the software compensations have been preferred in this study to reduce the burden of extra hardware.

The compensation for the digital delay is based on [13] while that for the inverter nonlinearity is based on [14]-[15]. However, in particular, the accurate compensation of the inverter nonlinearity is very difficult if the magnitude of the current is small because the influence of parasitic components, which is hard to expect, becomes dominant. In addition, even though the stator flux is not disappeared at standstill, its variation can be hard to detect in the proposed

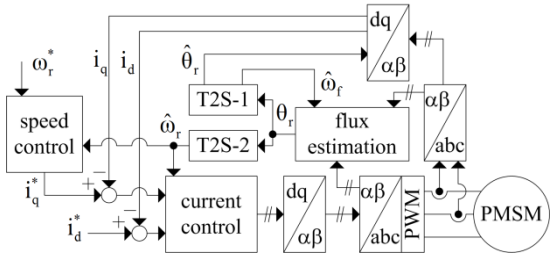

Fig. 5. Block diagram of proposed sensorless control system.

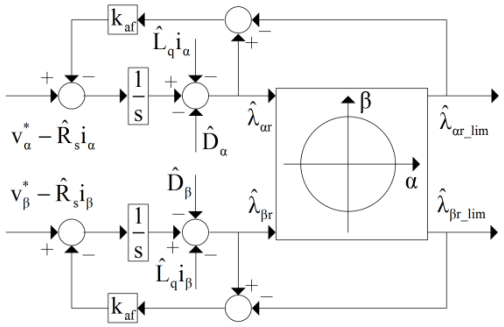

Fig. 6. Flux limiter at extremely low speed.

method if the stator current is not large enough. Then, the d-axis current is actively modulated in this paper to maintain a certain level of output current even under light loads. That is, the reliability of the proposed method can be improved at the expense of additional losses. The reference to the d-axis current can be generated according to (23) for the case of Surface Mounted PMSM (SMPMSM) if the q-axis current is smaller than a preset minimum level denoted by I_{min}:

$$i_d^* = \sqrt{I_{min}^2 - (i_q^*)^2} \ . \tag{23}$$

C. Limiter Design for Stator Flux Estimation

The integrands in (3) can have some errors due to sensing noises and parameter errors when the motor stands still. These types of errors cannot be negligible because they cause the integrators to diverge at standstill. The cumulative errors also can guide the estimated stator flux into incorrect direction, which means direct errors in the estimation of rotor angle. This would increase the failure rate of the sensorless drives if the motor has to be stopped for a while.

Practically, the rotor-oriented flux vector identified by $\lambda_{\alpha r}$ and $\lambda_{\beta r}$ in (6) is finite in its magnitude. That is, if the magnitude of the estimated flux vector is increasing without bound, it is definite that the estimated flux vector is going to somewhere else. The limiter in Fig. 6 has been inspired by this observation.

Because the flux limiter in Fig. 6 is proposed to be operated near zero speed, it is not activated simultaneously with k_{df} in Fig. 3. Then, the flux estimation in Fig. 5 is carried out by the block diagram of Fig. 6 near zero speed. The radius of the limiting circle in Fig. 6 can be set by considering λ_{em} in (5) with some margins. In order to set k_{af}

in Fig. 6, the following equation has been derived in the α–frame from Fig. 6:

$$\{v_\alpha^* - \hat{R}_s i_\alpha - k_{af}(\hat{\lambda}_{\alpha r} - \hat{\lambda}_{\alpha r\_lim})\}\frac{1}{s} - \hat{L}_q i_\alpha - \hat{D}_\alpha = \hat{\lambda}_{\alpha r}. \quad (24)$$

Equation (25) can be derived from (24):

$$\hat{\lambda}_{\alpha r} = \frac{k_{af}}{s + k_{af}}\left(\frac{v_\alpha^* - \hat{R}_s i_\alpha}{k_{af}} + \hat{\lambda}_{\alpha r\_lim}\right) - \frac{s}{s + k_{af}}(\hat{L}_q i_\alpha + \hat{D}_\alpha). \quad (25)$$

Considering (25), k_{af} works to make the estimated flux $\hat{\lambda}_{\alpha r}$ converge to the limited flux $\hat{\lambda}_{\alpha r\_lim}$. In order to set k_{af}, the following points should be considered. Initially, if k_{af} is largely set, the converging rate becomes high while the erroneous portion of $v_\alpha^* - \hat{R}_s i_\alpha$ in $\hat{\lambda}_{\alpha r}$ is decreased. However, too large k_{af} should be avoided because it can impede the detection of flux variation when the motor starts to rotate. Thus, the careful compromise is required to determine k_{af}.

V. Experiments

A. Experimental set-up

Even though the proposed method in this paper is also compatible with Interior PMSM (IPMSM), SMPMSM has been selected for practical assessment due to the following reasons. First, since the injection-based sensorless methods rely on the spatial saliency of inductance, the merit of the proposed method can be more obvious with SMPMSM, which has no saliency for the signal injection sensorless control. Second, the driving performance of IPMSM is also affected by how to control its reluctance torque. That is, because the sensorless control method is not the only factor to affect the driving performance, the evaluation of the performance of the sensorless control proposed in this study may be ambiguous with IPMSM. In addition, the strategy of (23), which is critical under light loads, can be simply applied in the case of SMPMSM without considering side effects.

To discuss the effectiveness of the proposed method, the practical system shown in Fig. 7 has been considered, where the ratings of the 8-pole SMPMSM are 11.5 N-m and 1500 r/min. The induction machine (IM) in Fig. 7(a) was employed to apply load torque to the SMPMSM during driving. Although a 5000 ppr encoder had been installed on the SMPMSM side, it was only used for the assessment of the proposed sensorless method. Namely, the measured angle and speed have never been allowed to help the proposed method.

The inverters in Fig. 7(b) were used to drive the motors, whose dc-link was rectified one from 3 phase–220 V_{rms} AC grid. The gating signals for the inverters were generated by a digital signal processor (DSP) board, which was based on TMS320F28335. For the digital control, the sampling frequency was set to 10 kHz while the switching frequency to 5 kHz. The preset dead-time was 2.5 μs. The voltage references, which are the outputs of the current controller, were synthesized by the space vector PWM (SVPWM) [16].

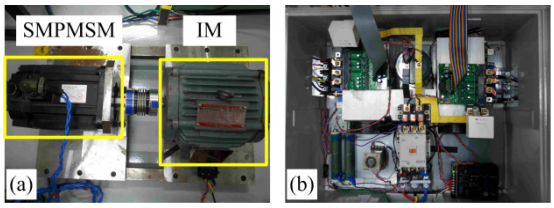

Fig. 7. Experimental set-up: (a) motors, (b) inverters.

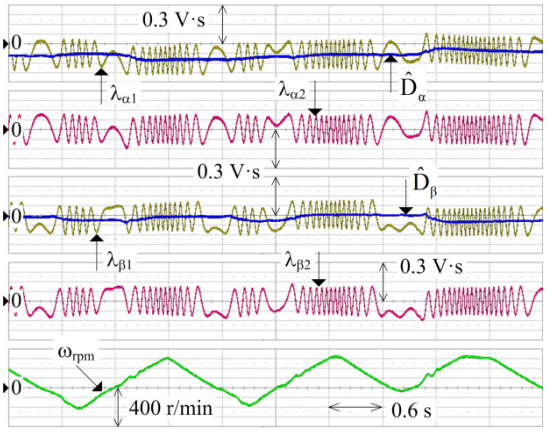

Fig. 8. Flux and disturbance estimations under 2 N-m load.

The bandwidths of the current and speed controls were set to 250 and 5 Hz, respectively. To estimate the rotor angle and speed, the bandwidth of T2S-1 in Fig. 5 was set to 60 Hz while that of T2S-2 to 35 Hz [11]. In order to refine the light load operations, I_{min} in (23) was set to 4 A when considering the distorted voltage from the inverter nonlinearity [14]. The radius of the limiting circle in Fig. 6 was set to 1.15 times the flux linkage under the consideration of λ_{em} in (5). For controls, the fixed values of R_s and L_q (=L_d) were used normally, which were respectively 0.327 Ω and 2.63 mH. In addition, if the estimated speed was larger than 1.5 Hz in electrical speed, k_{df} in Fig. 3 was activated with the value of 0.5. Otherwise, k_{af} in Fig. 6 was activated with the value of $2\pi \cdot 100$.

B. Experimental results

All of the following results were obtained when the test motor was under the speed control by the proposed sensorless method. Two four-channel oscilloscopes were used to gather experimental data, whose synchronization was achieved by observing the same waveform in both oscilloscopes.

Initially, the proposed flux estimation shown in Fig. 3 can be understood in its operation through Fig. 8. The flux and disturbance estimations are presented in the figure when the speed is arbitrarily reversed under 2 N-m load. Although the estimated speeds were used for the proposed method, the actual speed of ω_{rpm} has been captured to correctly inform the actual state. As shown in Fig. 8, the disturbances in $\lambda_{\alpha 1}$ and $\lambda_{\beta 1}$ seem to be effectively tracked by the proposed disturbance observer. As the result, the alternative variations of $\lambda_{\alpha 2}$ and $\lambda_{\beta 2}$, which are the main source of the information

to calculate the rotor angle by (6), appear with respect to zero almost all the time in Fig. 8.

In the experiment of Fig. 9, k_{df} in Fig. 3 was deactivated on purpose even though the rotating speed was not low enough to deactivate. After k_{df} is deactivated, $\lambda_{\alpha 1}$ and $\lambda_{\beta 1}$, estimated by the integrations, start to deviate from zero evidently. It is easily inferred that these fluxes can diverge if the feedback loop by k_{df} is not utilized. In addition, the abrupt activation of k_{df} may distort the estimation of $\lambda_{\alpha 2}$ and $\lambda_{\beta 2}$ when the motor escapes from extremely low speed range. Although this type of distortion from the reactivation is not severe in Fig. 9, it can be worsened with a smaller k_{df} that allows larger disturbances to be remained in $\lambda_{\alpha 1}$ and $\lambda_{\beta 1}$. Then, k_{df} should be properly set by considering (22) not to severely distort the flux estimation at its reactivation near zero speed.

The effect of the limiter described in Fig. 6 was discussed when the SMPMSM was driven under no load. In Fig. 10, through the signal of $FLAG_{limit}$, it can be recognized whether the proposed limiter operates or not. When $FLAG_{limit}$ was high near zero speed, the divergence of $\hat{\lambda}_{\alpha r}$ and $\hat{\lambda}_{\beta r}$ could be prevented by the proposed limiter as shown in Fig. 10. In result, the estimation error of rotor angle denoted by θ_d ($\theta_r - \hat{\theta}_r$) has not been diverged even at standstill.

The stable operation in Fig. 10 was possible because the setting in (23) was combined with the proposed limiter. By setting the d-axis current to be positive, the integrand errors in (3) at standstill could be integrated toward guiding the estimated rotor-oriented flux into the positive d-axis, at which the actual rotor flux must be oriented. When a negative value was assigned for the d-axis current instead, the driving system was always tripped. For the similar reason, it has been hard to stay at zero speed under heavy loads because the integrand errors were not directed to the positive d-axis. Unless the integrand errors are eliminated completely, the operation of motor at standstill must be limited.

The proposed sensorless method was examined under the speed reversal as shown in Fig. 11. In the speed reversal, if a sensorless control method works at crossing zero speed under heavier load with slower acceleration, it is regarded as the better one. The SMPMSM under test has revealed stable speed reversal responses at the variation of 90 r/min/s under 7.5 N-m load with the proposed method. As an example, the positive load condition was tested at increasing speed as shown in Fig. 11. If the speed was decreasing under a positive load, the speed control might be carried out by the load machine rather than the test motor. The effectiveness of the proposed method has been ascertained under the suitable conditions. The angle error θ_d was less than 0.25 rad near zero speed as shown in Fig. 11.

As explained earlier, the SMPMSM cannot be stopped indefinitely at standstill under heavy loads with the proposed method. However, as shown in Fig. 12, it has been confirmed that the test motor can be repeatedly stayed at standstill for 300 ms under 7.5 N-m load, which corresponds

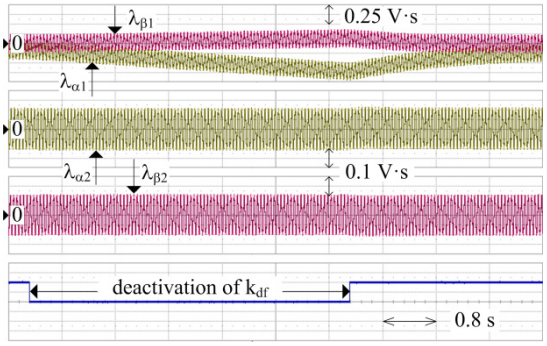

Fig. 9. Intentional deactivation of k_{df} at −300 r/min under −3 N-m load.

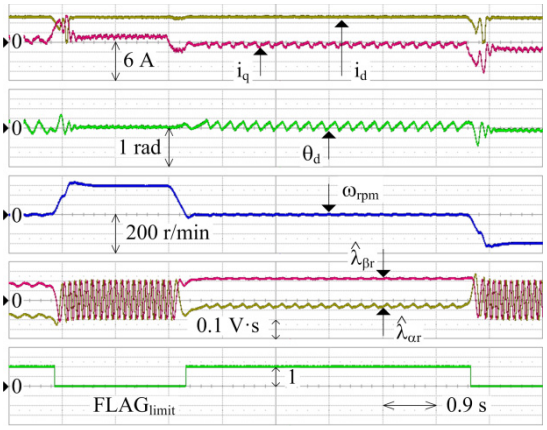

Fig. 10. No load operation.

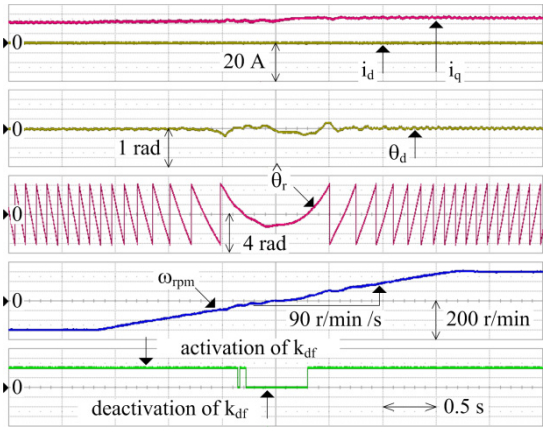

Fig. 11. Speed reversal under 7.5 N-m load.

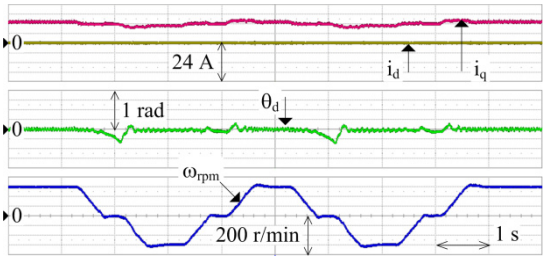

Fig. 12. Short stoppings at zero speed under 7.5 N-m load.

to 65.2 % of the rated torque. Since a certain degree of transient angle error is inevitable in the sensorless control

system, the maximum output torque insured by the sensorless control method had to be smaller than the original rated torque.

VI. CONCLUSION

The frequency-adaptive disturbance observer has been proposed in this paper to enhance the performance of the sensorless control method based on the stator flux model of PMSM. The state equation has been established for the observer, and it has been detailed how to set the observer gains with considering the speed reversal of PMSM. In addition, several auxiliary parts have been proposed to integrate the proposed observer into the sensorless control system under the consideration of practical measurement set-up of PMSM drive system. The feasibility of the proposed sensorless method has been scrutinized in an SMPMSM drive system coupled to an induction machine. Although the proposed method could not ensure its performance over all operating conditions, the speed of the test motor could be repeatedly reversed by the proposed method less than ±10 % of its rated speed under 65.2 % load. And the test motor can stay at zero speed with partial load without instability issues for several hundred milliseconds.

REFERENCES

[1] Y.-D. Yoon, S.-K. Sul, S. Morimoto and K. Ide, "High-Bandwidth Sensorless Algorithm for AC Machines Based on Square-Wave-Type Voltage Injection," *IEEE Trans. Ind. Appl.*, vol. 47, no. 3, May/June 2011.

[2] J. Holtz, "Sensorless Control of Induction Machines – With or Without Signal Injection?," *IEEE Trans. Ind. Electron.,* vol. 53, no. 1, pp. 7-30, Feb. 2006.

[3] R. Mizutani, T. Takeshita, N. Matsui, "Current Model-Based Sensorless Drives of Salient-Pole PMSM at Low Speed and Standstill," *IEEE Trans. Ind. Appl.*, vol. 34, no. 4, pp. 841-846, Jul./Aug. 1998.

[4] S. Morimoto, K. Kawamoto, M. Sanada, and Y. Takeda, "Sensorless Control Strategy for Salient-Pole PMSM Based on Extended EMF in Rotating Reference Frame," *IEEE Trans. Ind. Appl.,* vol. 38, no. 4, Jul./Aug. 2002.

[5] P. Kshirsagar, R. P. Burgos, J. Jang, A. Lidozzi, F. Wang, D. Boroyevich, and S.-K. Sul, "Implementation and Sensorless Vector-Control Design and Tuning Strategy for SMPM Machines in Fan-Type Applications," *IEEE Trans. Ind. Appl.*, vol. 48, no. 6, pp. 2402-2413, Nov./Dec. 2012.

[6] I. Boldea, M. C. Paicu, and G.-D. Andreescu, "Active Flux Concept for Motion-Sensorless Unified AC Drives," *IEEE Trans. Power Electron.*, vol. 23, no. 5, pp. 2612-2618, Sep. 2008.

[7] G. Foo, and M. F. Rahman, "Sensorless Direct Torque and Flux-Controlled IPM Synchronous Motor Drive at Very Low Speed Without Signal Injection," *IEEE Trans. Ind. Electron.*, vol. 57, no. 1, pp. 395-403, Jan. 2010.

[8] Z. Q. Zhu, and L. M. Gong, "Investigation of Effectiveness of Sensorless Operation in Carrier-Signal-Injection-Based Sensorless-Control Methods," *IEEE Trans. Ind. Electron.*, vol. 58, no. 8, pp. 3431-3439, Aug. 2011.

[9] Y. Park, S.-K. Sul, J.-K. Ji and Y.-J. Park, "Analysis of Estimation Errors in Rotor Position for a Sensorless Control System Using a PMSM," *Journal of Power Electron.*, vol. 12, no. 5, pp. 748-757, Sept. 2012.

[10] D. G. Luenberger, "An introduction to observers," *IEEE Trans. Automatic Control*, vol. 16, no. 6, pp. 596-602, Dec. 1971.

[11] Y. Park, S.-K. Sul, W.-C. Kim, and H.-Y. Lee, "Phase Locked Loop Based on an Observer for Grid Synchronization," in *Proc. IEEE Applied Power Electron. Conf. Exposition (APEC)*, Mar. 17-21, 2013, pp. 308-315.

[12] Y.-C. Son, B.-H. Bae, and S.-K. Sul, "Sensorless Operation of Permanent Magnet Motor Using Direct Voltage Sensing Circuit," in *Conf. Rec. IEEE IAS Annu. Meeting*, Oct. 13-18, 2002, pp. 1674-1678.

[13] B.-H. Bae and S.-K. Sul, "A Compensation Method for Time Delay of Full-Digital Synchronous Frame Current Regulator of PWM AC Drives," *IEEE Trans. Ind. Appl.*, vol. 39, no. 3, pp. 802-810, May/June 2003.

[14] Y. Park, and S.-K. Sul, "A Novel Method Utilizing Trapezoidal Voltage to Compensate for Inverter Nonlinearity," *IEEE Trans. Power Electron.*, vol. 27, no. 12, pp. 4837-4846, Dec. 2012.

[15] Y. Park and S.-K. Sul, "Compensation of Inverter Nonlinearity Based on Trapezoidal Voltage," in *Proc. IEEE Energy Convers. Congr. Exposition (ECCE),* Sept. 15-20, 2012, pp. 2292-2299.

[16] D.-W. Chung, J.-S. Kim and S.-K. Sul, "Unified Voltage Modulation Technique for Real-Time Three-Phase Power Conversion," *IEEE Trans. Ind. Appl.*, vol. 34, no. 2, pp. 374-380, Mar./Apr. 1998.